



Cite this: DOI: 10.1039/c6dt04413a

# Single-molecule magnet behaviour in a tetranuclear Dy<sup>III</sup> complex formed from a novel tetrazine-centered hydrazone Schiff base ligand†

T. Lacelle,<sup>a</sup> G. Brunet,<sup>a</sup> A. Piat,<sup>a</sup> R. J. Holmberg,<sup>a</sup> Y. Lan,<sup>b</sup> B. Gabidullin,<sup>a</sup> I. Korobkov,<sup>a</sup> W. Wernsdorfer<sup>b,c,d</sup> and M. Murugesu<sup>\*a</sup>

Two analogous tetranuclear lanthanide complexes have been synthesized with the general formula [Ln<sub>4</sub>(vht)<sub>4</sub>(MeOH)<sub>8</sub>](NO<sub>3</sub>)<sub>4</sub>·aMeOH·bH<sub>2</sub>O, where H<sub>2</sub>vht = (3,6-bis(vanillidenehydrazinyl)-1,2,4,5-tetrazine) and Ln = Dy<sup>III</sup> (**1**), Gd<sup>III</sup> (**2**). These complexes are characterized by several techniques; including single-crystal X-ray diffraction, SQUID magnetometry and single-crystal micro-SQUID hysteresis loop measurements. Elucidation of the crystal structure of the complexes shows that the lanthanide ions are bridged by a tetrazine ring, a rare bridging moiety for lanthanide ions. Magnetic studies reveal that both **1** and **2** exhibit weak ferromagnetic exchange interactions between Ln ions, and **1** displaying Single-Molecule Magnet (SMM) behaviour with a magnetisation reversal barrier of  $U_{\text{eff}} = 158 \text{ K}$  ( $\tau_0 = 1.06 \times 10^{-7} \text{ s}$ ).

Received 21st November 2016,  
Accepted 14th January 2017

DOI: 10.1039/c6dt04413a

rsc.li/dalton

## Introduction

Tetrazines, particularly 1,2,4,5-tetrazines, have been employed in numerous fields of scientific research, ranging from coordination chemistry to energetic materials.<sup>1</sup> Tetrazines have even been shown to have biological applications through their ability to undergo rapid inverse electron-demand Diels–Alder reactions.<sup>2</sup> Primarily, interest in tetrazines stems from their unique structural and electrochemical properties.<sup>3</sup> The four N-atoms in the tetrazine ring result in a remarkably low-lying  $\pi^*$  orbital, resulting in tetrazines being strong  $\pi$ -acceptors and having low one electron reduction potentials (typically  $E > -1.3 \text{ V}$  vs. ferrocene) toward the formation of radical anions.<sup>1</sup> In addition, these N-donors enable tetrazines to be excellent bridging ligands in polynuclear complexes.<sup>4</sup> Recent results from Dunbar and co-workers on a tetrazine-based complex show remarkable magnetic properties with large exchange coupling constants between Co<sup>II</sup> ions and the anion

radical of a tetrazine,<sup>5</sup> illustrating that tetrazines can be used to promote strong magnetic exchange interactions.

In order to implement tetrazines into our systems, we resorted to a Schiff base motif in our ligand design. The chemistry of Schiff bases offers a wide variety of potential ligands through their high degree of tunability. The availability of numerous keto and amino precursors presents a great opportunity for synthesizing imine compounds with varying structural properties. Careful selection of the precursors allows for the control of denticity, size/shape of binding sites, as well as any desired moieties to be incorporated into the ligand. Thus, our research efforts revolved around implementing a tetrazine ring as a functional moiety of a Schiff base ligand, allowing for the design of polynuclear lanthanide complexes.

Through the introduction of tetrazines into Schiff-base ligands, we are able to access a largely unexplored field. There has been only one previously reported structure composed of a Schiff base ligand containing a tetrazine moiety; Roberts and co-workers reported Fe<sub>4</sub> tetrahedral cages which underwent post-assembly modification through inverse electron-demand Diels–Alder reactions.<sup>6</sup> Tetrazine-based bridging systems, particularly with lanthanides, are also rare in the literature. The oxophilic nature of the lanthanide ions, combined with the weak  $\sigma$ -donating character of tetrazines, presents a great challenge for synthesizing tetrazine-based lanthanide compounds. To the best of our knowledge Ward and co-workers reported the only two examples of tetrazine-bridged lanthanide complexes, which were found to act as near-infrared emitters.<sup>7</sup> In order to isolate multinuclear complexes with new structural topologies and interesting magnetic properties, we situated

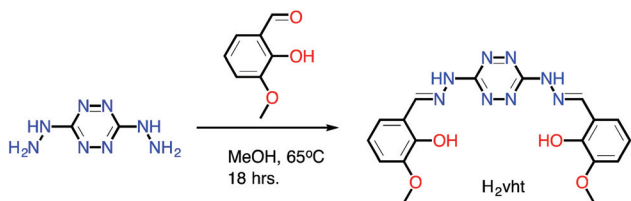
<sup>a</sup>Department of Chemistry and Biomolecular Sciences, University of Ottawa, 10 Marie Curie, Ottawa, ON K1N 6N5, Canada. E-mail: m.murugesu@uottawa.ca

<sup>b</sup>Institut Néel, CNRS and Université Grenoble Alpes, BP 166, 25 Avenue des Martyrs, 38042 Grenoble, France

<sup>c</sup>Physikalisches Institut, Karlsruhe Institute of Technology (KIT), Wolfgang-Gaede Str. 1, D-76131 Karlsruhe, Germany

<sup>d</sup>Institut für Nanotechnologie, Karlsruhe Institute of Technology (KIT), Hermann-von-Helmholtz Platz 1, D-76344 Eggenstein-Leopoldshafen, Germany

† Electronic supplementary information (ESI) available: Detailed experimental procedures, CIF files and supporting figures. CCDC 1518373–1518375. For ESI and crystallographic data in CIF or other electronic format see DOI: 10.1039/c6dt04413a



**Scheme 1** Synthesis of  $H_2vht$ .

the tetrazine ring as an integral part of the ligand coordination pockets, which contain donor atoms with higher Lewis basicity to enable the tetrazine to act as a bridge between metal ions through chelation (Scheme 1).

With these principles in mind, we focused our attention on tetrazines as a bridging motif to probe the nature and strength of the magnetic interactions between lanthanide ions. The large unquenched orbital angular momentum exhibited by lanthanide ions, such as  $Dy^{III}$ , gives rise to magnet-like behavior in many lanthanide complexes in the form of slow relaxation of the magnetisation. Discrete molecules that demonstrate this slow relaxation are referred to as Single-Molecule Magnets (SMMs). These systems have vast potential applications in several high-tech disciplines such as ultra-high density data storage, spintronic devices as well as next-generation MRI contrast agents.<sup>8</sup> Herein, we report a unique system consisting of two tetranuclear lanthanide complexes based on anisotropic  $Dy^{III}$  (**1**) and isotropic  $Gd^{III}$  (**2**) metal ions. Complex **1** exhibits slow relaxation of the magnetisation, making **1** the first tetrazine-bridged SMM under zero applied field.

## Experimental

### Materials

All chemicals were of reagent grade, purchased from TCI, Alfa Aesar and Strem Chemicals and were used without any further purification.

### Elemental analysis, IR, UV-VIS, NMR spectroscopy

Elemental analysis was performed using an Isotope Cube elemental analyser. Infrared spectra were obtained with a Varian 640 FTIR spectrometer equipped with an ATR in the  $4000\text{ cm}^{-1}$  to  $600\text{ cm}^{-1}$  range. UV-VIS spectra were measured using an Agilent Cary 5000 UV-VIS-NIR spectrometer in the range of 200 to 800 nm. All samples were measured in MeOH using a standard 10 mm pathlength cuvette. NMR analyses were carried out using a Bruker Avance 400 spectrometer equipped with an automated sample holder and a 5 mm auto-tuning broadband probe with  $Z$  gradient.

### Synthesis of (3,6-bis(vanillidenehydrazinyl)-1,2,4,5-tetrazine), $H_2vht$

The precursor, 3,6-bis(hydrazinyl)-1,2,4,5-tetrazine, was synthesized according to a previously reported procedure with slight modifications (Scheme S1†).<sup>9</sup> To a suspension of 3,6-bis-

(hydrazinyl)-tetrazine (4.00 g, 0.028 mol) in methanol (500 mL) was added *o*-vanillin (9.47 g, 0.062 mol) (Scheme 1). The resulting reaction mixture was stirred under reflux over 18 h and then was allowed to cool to room temperature. The red precipitate was collected by filtration and washed with methanol. Recrystallization from DMF yields the DMF solvate of  $H_2vht$  as dark red needle-shaped crystals suitable for single-crystal X-ray diffraction. The crystalline material was collected by suction filtration and dried under vacuum prior to its use as the ligand (5.85 g, 0.014 mol, 51%). <sup>1</sup>H NMR (DMSO- $d_6$ , 400 MHz)  $\delta$  3.78 (s, 6H, OCH<sub>3</sub>), 6.82 (t,  $J = 7.9$  Hz, 2H, Ar), 6.96 (dd,  $J = 7.9$  and 1.4 Hz, 2H, Ar), 7.10 (dd,  $J = 7.9$  and 1.4 Hz, 2H, Ar), 8.41 (s, 2H, N=CH), 10.73 (s, 2H, NH), 12.05 (s, 2H, OH); <sup>13</sup>C (DMSO- $d_6$ , 100 MHz)  $\delta$  160.0, 148.4, 147.0, 144.5, 120.8, 119.9, 119.5, 113.7, 56.3. IR (ATR,  $\text{cm}^{-1}$ ): 3207 (br), 2980 (br), 1569 (m), 1538 (m), 1463 (m), 1417 (s), 1385 (m), 1366 (m), 1281 (w), 1247 (s), 1147 (m), 1094 (m), 1079 (m), 1043 (s), 982 (m), 940 (m), 885 (w), 856 (w), 833 (w), 781 (m), 736 (s), 633 (m), 585 (w), 565 (m). Elemental analysis; Expected: C 52.68%, H 4.42%, N 27.30%; Found: C 51.96%, H 4.54%, N 27.35%.

**Synthesis of  $[Dy_4(vht)_4(MeOH)_8](NO_3)_4 \cdot 8.07MeOH \cdot 0.65H_2O$  (**1**).** A room temperature suspension of  $Dy(NO_3)_3 \cdot 6H_2O$  (114 mg, 0.25 mmol) and  $H_2vht$  (51 mg, 0.125 mmol) in MeOH was stirred for 5 min, after which  $NaN_3$  (16 mg, 0.25 mmol) was added. The reaction mixture was stirred for another 30 minutes, filtered, and the filtrate was left to stand in a sealed vial. After 2 days, black block-shaped crystals suitable for single-crystal X-ray diffraction were obtained. Yield = 33%. IR (ATR,  $\text{cm}^{-1}$ ): 3201 (br), 2941 (w), 2832 (w), 1603 (m), 1573 (m), 1524 (m), 1447 (m), 1397 (m), 1310 (m), 1283 (m), 1239 (m), 1220 (s), 1169 (m), 1078 (m), 1055 (m), 1034 (m), 964 (m), 911 (w), 849 (m), 826 (w), 784 (w), 767 (w), 735 (s), 657 (m), 627 (m). UV-VIS spectra of **1**, **2** and  $H_2vht$  are depicted in Fig. S1.† Elemental analysis; Expected: C 34.59%, H 4.27%, N 16.49%; Found: C 34.21%, H 4.06%, N 16.97%.

**Synthesis of  $[Gd_4(vht)_4(MeOH)_8](NO_3)_4 \cdot 8.19MeOH \cdot 0.91H_2O$  (**2**).** The same procedure as **1** was employed to synthesize **2**, however, the metal salt was replaced by  $Gd(NO_3)_3 \cdot 6H_2O$  (113 mg, 0.25 mmol) to yield black block-shaped crystals suitable for single-crystal X-ray diffraction. Yield = 35%. IR (ATR,  $\text{cm}^{-1}$ ): 3211 (br), 2941 (w), 2832 (w), 1606 (m), 1585 (m), 1530 (m), 1447 (m), 1397 (m), 1316 (m), 1287 (m), 1239 (m), 1220 (s), 1168 (m), 1114 (m), 1077 (m), 1056 (m), 1013 (m), 967 (m), 910 (w), 851 (m), 826 (w), 784 (w), 768 (w), 737 (s), 659 (m), 630 (m). Elemental analysis; Expected: C 34.77%, H 4.32%, N 16.56%; Found: C 34.36%, H 4.10%, N 16.74%.

### Single-crystal X-ray diffraction analysis

The crystals were mounted on a thin glass fibre using paraffin oil. Prior to data collection crystals were cooled to 200 K. Data were collected on a Bruker AXS SMART single-crystal diffractometer equipped with a sealed Mo tube source ( $\lambda = 0.71073\text{ \AA}$ ) APEX II CCD detector. Raw data collection and processing were performed with the APEX II software package from BRUKER AXS.<sup>10</sup> Semi empirical absorption corrections based on equivalent reflections were applied.<sup>11</sup> Direct methods

yielded all non H-atoms, which were refined with anisotropic thermal parameters. All hydrogen atoms were calculated geometrically and were riding on their respective atoms. Crystallographic data for the ligand **H<sub>2</sub>vht**, **1** and **2** are depicted in Table S1.† CCDC numbers are as follows: 1518373 (**1**), 1518374 (**2**), 1518375 (**H<sub>2</sub>vht**).

### Magnetic measurements

Magnetic susceptibility measurements were performed using a MPMS-XL7 Quantum Design SQUID magnetometer. Direct current (dc) susceptibility data measurements were performed at temperatures ranging from 1.9 to 300 K, and between applied fields of  $-5$  to  $5$  T. Measurements were performed on crushed polycrystalline samples with 24.6 and 23.4 mg for samples **1** and **2**, respectively. Each sample was wrapped in a polyethylene membrane. Alternating current (ac) susceptibility measurements were performed under an oscillating ac field of 3.78 Oe and ac frequencies ranging from 0.1 to 1500 Hz. Magnetisation *vs.* field measurements were performed at 100 K in order to check for the presence of ferromagnetic impurities, which were found to be absent. Magnetic data were corrected for diamagnetic contributions using Pascal's constants.

## Results and discussion

### Structural details

In order to give a detailed description of the structural characteristics of the free ligand, and to observe the effects of coordination, single-crystal X-ray diffraction was carried out on the **H<sub>2</sub>vht** ligand, in addition to NMR spectroscopy. The ligand crystallizes in the monoclinic  $P2_1/c$  space group with all of the ligand atoms being nearly coplanar. The structure of the ligand consists of one central tetrazine ring and two identical hydrazone substituents derived from *o*-vanillin (Fig. 1). The molecule exhibits centrosymmetry with the inversion center located directly in the center of the tetrazine ring. The two vanillidene moieties, in conjunction with the tetrazine ring, form four coordination pockets. These pockets are comprised of two large tridentate pockets consisting of N1, N4a and O1 and two smaller bidentate pockets formed by O1 and O2 from the vanillidene moieties. The larger pockets are well-suited to

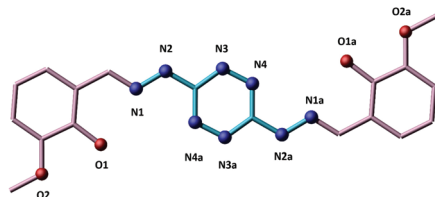


**Fig. 1** Crystal structure of **H<sub>2</sub>vht** (3,6-bis(vanillidenehydrazinyl)-1,2,4,5-tetrazine). Solvent molecules and hydrogen atoms were omitted for clarity. Symmetry equivalent atoms are denoted by an additional "a" in the label. Colour code: red (O), blue (N). All unfilled vertices are carbon atoms.

the encapsulation of lanthanide ions. The N–N bond lengths of 1.32 Å and C–N bond lengths of 1.34 Å are in agreement with previously reported tetrazine compounds.<sup>12</sup> The <sup>1</sup>H NMR spectrum of **H<sub>2</sub>vht** consists of four singlets and three phenyl multiplets. The full spectrum of **H<sub>2</sub>vht** is depicted in Fig. S2.†

Coordination of the deprotonated ligand to Dy<sup>III</sup> or Gd<sup>III</sup> yields two isostructural complexes, with the Dy<sup>III</sup> complex (**1**) depicted in Fig. 2. The complexes crystallize in the triclinic  $P\bar{1}$  space group. For brevity, the Dy analogue will be described. Each Dy<sup>III</sup> ion adopts an ennea-coordinate motif, with three N-donors and six O-donors. For example, Fig. 2 shows that Dy1 is coordinated to two imine nitrogen atoms, N8 and N9, and one nitrogen from the tetrazine ring, N11. The *o*-vanillin side groups contribute oxygen atoms O1, O2, O3 and O5 to the coordination sphere of Dy1. Two oxygen atoms from two methanol molecules, O15 and O16, make up the remainder of the coordination sphere. Dy2 exhibits a similar coordination environment to Dy1. The comparison of thirteen reference

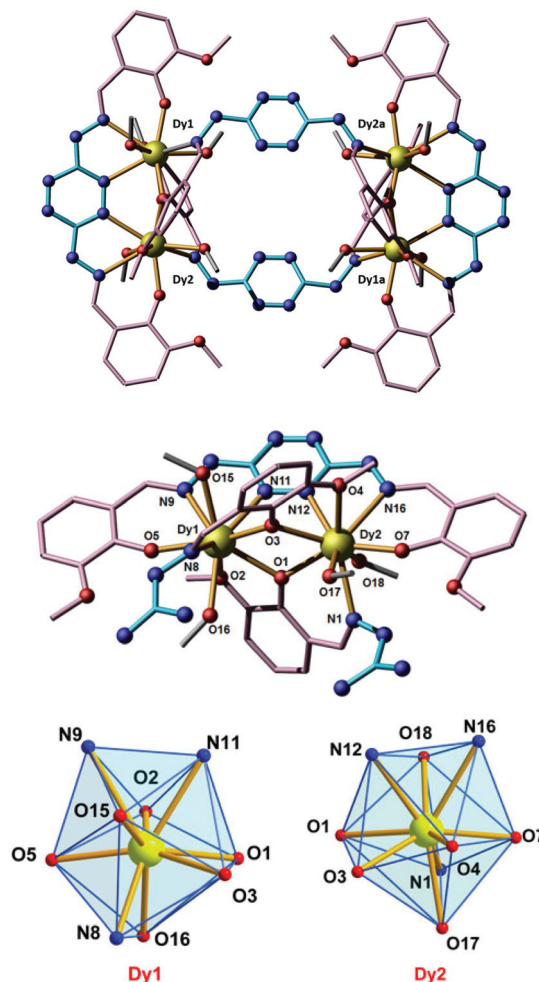


**Fig. 2** Molecular structure (top), dinuclear subunit (middle) and coordination polyhedra (bottom) for complex **1**. Colour code: yellow (Dy), red (O), blue (N). Hydrogen atoms are omitted for clarity. All unfilled vertices are carbon atoms.

polyhedra with the coordination polyhedra of Dy1 and Dy2 by SHAPE analysis<sup>13</sup> (Table S2†) reveals that Dy1 possesses a distorted spherical capped square antiprism ( $C_{4v}$ ) geometry while Dy2 resembles a spherical tricapped trigonal prism ( $D_{3h}$ ) (Fig. 2). It is also important to note that the cationic complexes are charge balanced by four nitrate anions, some of which exhibit partial occupancies (N18 and N19). Moreover, a significant amount of lattice solvent molecules can be found; most notable is the presence of roughly 8 MeOH molecules (8.07 and 8.19, for **1** and **2**, respectively), along with a smaller contribution of water molecules (0.65 and 0.91 for **1** and **2**, respectively). Thus, while manipulating the crystals of **1** and **2**, care must be taken to prevent evaporation of the solvent molecules, which causes visible cracking of the crystals.

While complexes **1** and **2** are tetranuclear overall, they are composed of two dinuclear subunits (Fig. 2). These subunits are linked by two ligand molecules and bound by the vanillidene donor atoms. This bridging motif between subunits also provides two bridging modes between Dy1 and Dy2 in the form of phenoxide oxygen atoms, O1 and O3. With the two phenoxide atoms and the tetrazine ring there is a total of three bridging motifs between the Dy<sup>III</sup> centers.

In addition, the complex is also centrosymmetric, giving rise to symmetry equivalent atoms between subunits. While the dinuclear lanthanide complexes of Shavaleev and co-workers do possess a tetrazine bridge,<sup>7</sup> the lanthanide ions are bridged from across the tetrazine moiety. In the case of complexes **1** and **2**, the Ln<sup>III</sup> ions are bridged by the tetrazine ring from the same side. This leads to an unprecedented bridging motif for lanthanide-based systems. Another distinguishing feature in our system is the large spatial separation between the dinuclear subunits with a Dy1–Dy2a distance of 10.49 Å and a Dy1–Dy1a distance of 11.21 Å. For comparison, the smallest intermolecular Dy...Dy distance for complex **1** is 10.43 Å. These distances are significantly larger than those of the Dy1–Dy2 subunit distances of 3.91 Å. Statistical analysis for all reported compounds with Dy<sup>III</sup> ions bridged by moieties consisting of one or two atoms shows that the average intramolecular Dy...Dy distance is 3.83 Å. The Dy1–Dy2 distance of **1** is then slightly above the average intramolecular distances for similarly bridged compounds.

When comparing the free ligand to the coordinated tetrazine moiety, the latter exhibits a relatively large contortion of the tetrazine ring. The bond distance of the nitrogen atoms N11 and N12 in complex **1** is elongated to 1.36 Å while the opposite nitrogen atoms, N13 and N14, have a shorter bond distance of 1.27 Å (Fig. 3). The coordination of Dy<sup>III</sup> is likely the cause of this contortion, resulting in the ligand being forced outward from the metal ions.

### Static magnetic susceptibility

The analysis of the crystal structure of compounds **1–2** (*vide supra*) suggests that the most likely intramolecular magnetic interactions would occur between Ln1 and Ln2 of each subunit. This is due to the close proximity of these metal ions (3.91 Å). Conversely, the two dinuclear subunits are well separ-

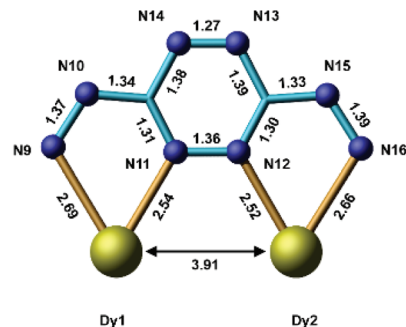


Fig. 3 Bond distances of the central tetrazine moiety of **1** in Å. Colour code: yellow (Dy), blue (N). Hydrogen atoms are omitted for clarity. All unfilled vertices are carbon atoms.

ated by distances of 10.49 Å and 11.21 Å, and thus are unlikely to experience any significant interaction between spin carriers. Close inspection of the bridging between Ln ions within a single dimer reveals the potential for three superexchange pathways. Two of the pathways are mediated by phenoxide moieties of the **H<sub>2</sub>vht** ligand, in a similar fashion to previously reported Schiff-base compounds,<sup>14</sup> while an additional bridging occurs through two nitrogen atoms (N11 and N12) of the tetrazine ring. It is important to note that dipole–dipole interactions will also likely contribute to the Ln<sup>III</sup>–Ln<sup>III</sup> coupling, in addition to the superexchange interactions like in most cases of lanthanide systems.

The temperature dependence of the  $\chi T$  product displays the presence of non-negligible ferromagnetic coupling between spin carriers (Fig. 4). The room temperature values at 300 K are 55.81 and 30.81 cm<sup>3</sup> K mol<sup>-1</sup> for **1** and **2**, respectively, which are in good agreement with the expected theoretical values of 56.68 and 31.52 cm<sup>3</sup> K mol<sup>-1</sup>, for four non-interacting lanthanide ions (Dy<sup>III</sup>: <sup>6</sup>H<sub>15/2</sub>,  $S = 5/2$ ,  $L = 5$ ,  $g = 4/3$ ;

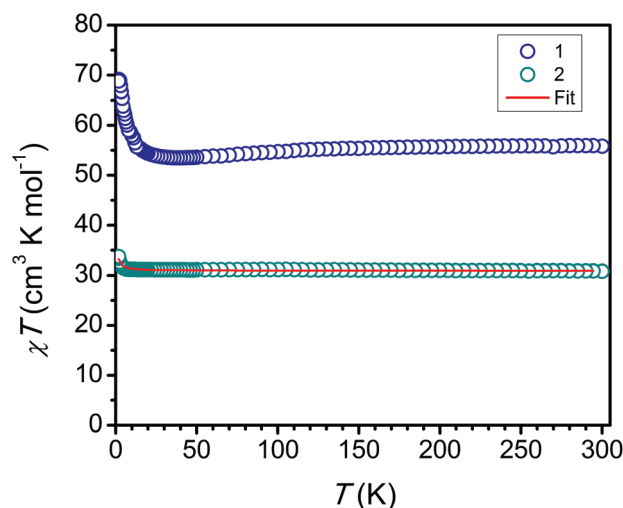


Fig. 4  $\chi T$  vs.  $T$  plot for **1** and **2** under applied dc fields of 1000 Oe. The solid line shows the best fit obtained through the magnetic model described in the text.

Gd<sup>III</sup>:  $^8S_{7/2}$ ,  $S = 7/2$ ,  $L = 0$ ,  $g = 2$ ). Upon lowering the temperature, the  $\chi T$  values of **1** and **2** remain relatively constant down to 12 K, before abruptly increasing to a maximum of 69.86 cm<sup>3</sup> K mol<sup>-1</sup> for **1** and 33.73 cm<sup>3</sup> K mol<sup>-1</sup> for **2** at 1.9 K. This sharp increase is indicative of intramolecular ferromagnetic coupling, which dominates the magnetic behaviour at low temperatures. In order to further probe the magnetic exchange interactions, we applied the Van Vleck equation to Kambe's vector coupling scheme using the isotropic spin Hamiltonian:

$$\hat{H} = -2J(\hat{S}_a \cdot \hat{S}_b + \hat{S}_a \cdot \hat{S}_b)$$

with  $S_a = S_b = 7/2$ , allowing us to reproduce the  $\chi T$  curve of **2** (Fig. 4). Due to the symmetry equivalence of the dimeric subunits and their spatial separation with respect to each other we decided to model the exchange interactions of **2** with one  $J$  parameter. The best-fit parameters obtained were  $J = 0.009(3)$  cm<sup>-1</sup> and  $g = 1.982(1)$ , testifying the weak ferromagnetic interactions between lanthanide ions.<sup>14</sup> As noted above, these interactions likely originate from superexchange and dipole-dipole interactions. It is also important to note that there is a greater upturn in the  $\chi T$  product of **1**, which suggests that the interaction in **1** could be significantly larger than that in **2**.

Furthermore, we examined the field ( $H$ ) dependence of the magnetisation ( $M$ ), which shows a rapid increase of the magnetisation at low fields up to 27.40  $\mu_B$  (**1**) and 25.49  $\mu_B$  (**2**) at 5 T and 2.0 and 1.9 K, respectively (Fig. S3†). This rapid increase in magnetisation is expected for ferromagnetically coupled systems.<sup>15</sup> The  $M$  vs.  $HT^{-1}$  plots, at varying temperatures, show magnetisation curves that are slightly deviated from one another, suggesting the presence of non-negligible magneto-anisotropy and/or low-lying excited states for compound **1** (Fig. S4†). On the other hand, the isotropic nature of **2** is confirmed through the superimposition of the analogous magnetisation curves at differing temperatures (Fig. S4†).

### Dynamic magnetic susceptibility

Due to the recent successes of discrete Dy-based complexes displaying record SMM properties,<sup>16</sup> we were prompted to investigate the dynamics of the magnetisation of compound **1**. The frequency dependence of the ac susceptibility was investigated under zero applied dc field (Fig. 5). The  $\chi''$  vs.  $\nu$  data for **1** were fitted using a generalized Debye model for a single relaxation process:<sup>17</sup>

$$\chi'(\nu) = \chi_s + (\chi_T - \chi_s) \frac{1 + (2\pi\nu\tau)^{1-\alpha} \sin\left(\frac{\pi\alpha}{2}\right)}{1 + 2(2\pi\nu\tau)^{1-\alpha} \sin\left(\frac{\pi\alpha}{2}\right) + (2\pi\nu\tau)^{2(1-\alpha)}}$$

$$\chi''(\nu) = (\chi_T - \chi_s) \frac{(2\pi\nu\tau)^{1-\alpha} \cos\left(\frac{\pi\alpha}{2}\right)}{1 + 2(2\pi\nu\tau)^{1-\alpha} \sin\left(\frac{\pi\alpha}{2}\right) + (2\pi\nu\tau)^{2(1-\alpha)}}$$

where  $\chi_T$  and  $\chi_s$  are the isothermal and adiabatic susceptibilities, respectively,  $\tau$  is the relaxation time and  $\alpha$  depicts the distribution of relaxation times. From these data, we can also observe frequency dependence in both the in-phase ( $\chi'$ ) and out-of-phase ( $\chi''$ ) signals. Selected data, including  $\tau$  and  $\alpha$

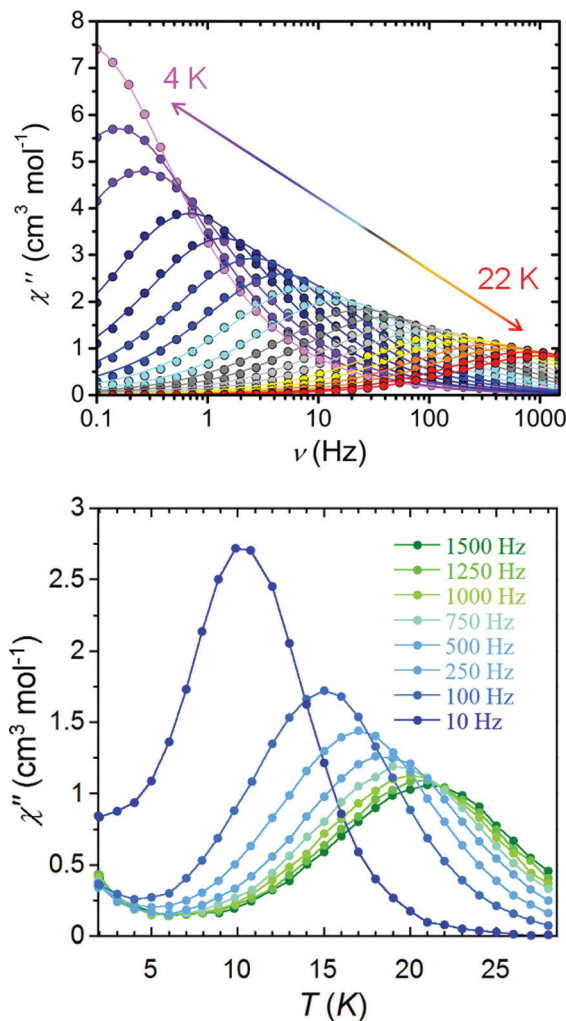


Fig. 5 Out-of-phase magnetic susceptibility ( $\chi''$ ) vs. frequency (top) and out-of-phase magnetic susceptibility vs. temperature (bottom) for **1**. The  $\chi''$  vs.  $\nu$  data for **1** were fitted using a generalized Debye model for a single relaxation process.

values obtained from the fits of  $\chi''$  vs.  $\nu$  are summarized in Table S3.† The shifting of peak maxima confirms slow relaxation of the magnetisation. The relaxation time ( $\tau$ ) is derived from the frequency dependent measurements between 5 and 18 K and plotted as a function of  $1/T$  (Fig. S5†). Above 15 K, the relaxation follows a thermally activated mechanism, eliciting an energy barrier of 158 K and a pre-exponential factor ( $\tau_0$ ) of  $1.06 \times 10^{-7}$  s using the Arrhenius equation:  $\tau = \tau_0 \exp(U_{\text{eff}}/kT)$ .

A graphical representation of  $\chi''$  vs.  $\chi'$  (Cole-Cole plot) for **1** was fitted using a generalized Debye model for a single relaxation process between 7 and 20 K (Fig. 6). The semi-circular plots give a moderately narrow distribution of  $\alpha$  parameters ranging from 0.25 to 0.41, which is consistent with the  $\alpha$  values obtained by fitting the frequency dependent data (Table S3†). The temperature dependence of the ac susceptibility was also investigated under zero applied dc field (Fig. 5).

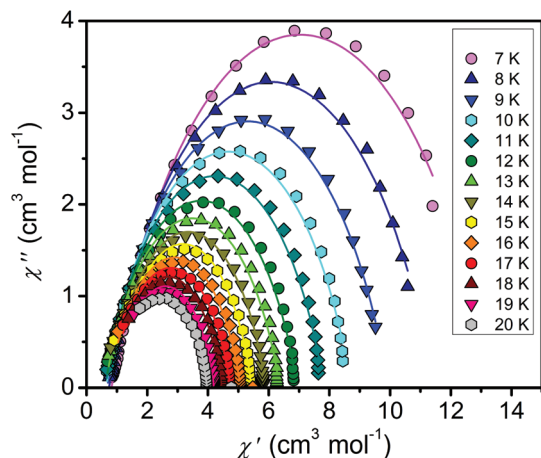


Fig. 6 Cole–Cole plot for frequency dependent ac susceptibility data of **1**. Solid lines are the best fit to the generalized Debye model.

The temperature dependence of the ac susceptibility under zero dc field reveals an out-of-phase signal ( $\chi''$ ) with observable maxima. As the frequency is increased, the maxima are shifted to higher temperatures, confirming slow relaxation of the magnetisation, characteristic of SMMs.

To further investigate the low temperature magnetic behaviour of complex **1**, single-crystal relaxation measurements were carried out on a micro-SQUID array.<sup>18</sup> Below 0.5 K at a sweep rate of 0.14 T s<sup>-1</sup>, the  $M$  vs.  $H$  sweeps exhibited hysteretic behaviour and a small opening could be observed up to a temperature of 4 K (Fig. 7). The width of the magnetic hysteresis loop of **1** shows strong temperature, and moderate sweep rate, dependence. The S shape of the hysteresis loop and the step position located between 0 and 0.2 T are reminiscent of previously reported weakly coupled lanthanide dimers. Such signature behaviours result from single-ion relaxation entangled with the neighbouring Dy ion relaxation within the molecule *via* weak intramolecular-exchanged biased interactions.<sup>14b</sup>

Electrostatic modelling of the anisotropy axes in complex **1** was also carried out using Magellan.<sup>19</sup> In the case of low symmetry Dy<sup>III</sup> complexes the ground Kramers doublet shows strong axiality and the  $g$ -tensor approaches that of the  $m_j = 15/2$  levels, where  $g_x = g_y = 0$  and  $g_z = 20$ .<sup>20</sup> The electron density distribution in Dy<sup>III</sup> can be approximated by an oblate spheroid, and by solving the electrostatic energy minimum with respect to the crystal field potential, the orientation of the magnetic anisotropy axes can be obtained. Carrying out this electrostatic modelling reveals a near-collinear alignment of the easy-axis vectors between Dy<sup>III</sup> centers (Fig. 8), with an angle of 7° between the Dy1 and Dy2 axes. The vectors lie along the direction of the anionic phenoxide atoms for each subunit, with deviations in the alignment of these vectors attributed to slight differences in the coordination geometry between the Dy1 and Dy2 ions. The centrosymmetry of the complex results in the antiparallel alignment of the easy axis vectors between the dinuclear subunits. Despite this antiferromagnetic alignment, the ferromagnetic interaction between

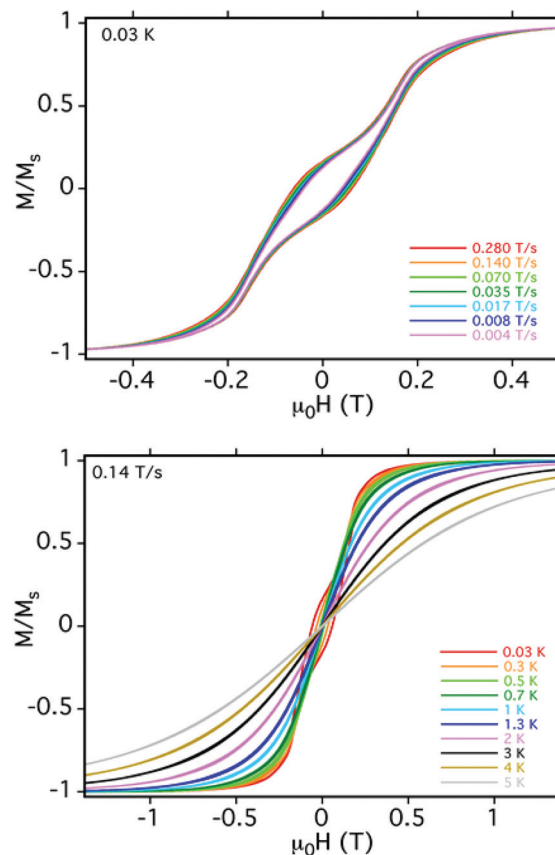


Fig. 7 Single-crystal magnetic hysteresis loop measurements on a micro-SQUID array for **1** with varying sweep rates (top) and temperatures (bottom).

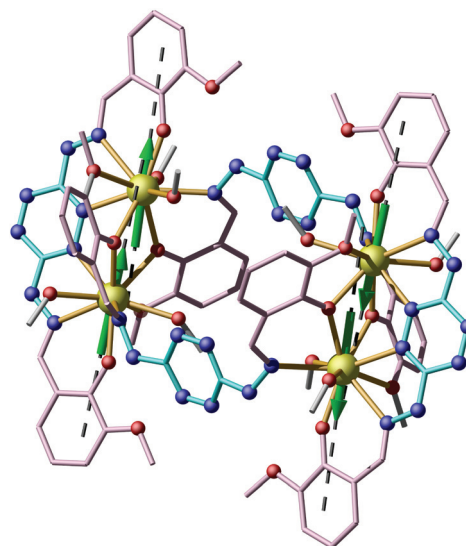


Fig. 8 Anisotropy axes in the ground Kramers doublet ( $m_j = 15/2$ ) for each Dy<sup>III</sup> ion in **1**. Axes modelled using Magellan software. Colour code: yellow (Dy), red (O), blue (N). Hydrogen atoms are omitted for clarity. All unfilled vertices are carbon atoms.

Dy1 and Dy2 is shown to be dominant due to the comparatively short intramolecular distance of 3.91 Å.

## Conclusions

The structural and magnetic properties of two analogous tetranuclear lanthanide complexes consisting of two dimeric subunits are presented and discussed. The synthesis of these complexes was achieved using a new compartmental Schiff base ligand incorporating a tetrazine ring. Both the Dy and Gd analogues exhibit dominant ferromagnetic exchange interactions at low temperature. The  $\{Ln_2\}$  subunits of these tetranuclear complexes are sufficiently separated to be treated as individual dinuclear systems and can therefore be modelled as such. In addition to exhibiting ferromagnetic exchange, compound **1** exhibits SMM behaviour with a sizeable magnetisation reversal barrier of 158 K. Although the strength of the interaction is weak, it is noteworthy that in this system dominant ferromagnetic interactions are observed. If such ferromagnetically coupled systems are strongly coupled, high spin ground states with large energy barriers can be expected. With this in mind our ongoing studies focus on the reduction of the tetrazine ring in order to improve the strength of the  $Ln^{III}$ – $Ln^{III}$  interactions through radical exchange coupling.

## Acknowledgements

We would like to thank the University of Ottawa, NSERC, CFI, and ORF for financial support.

## References

- (a) W. Kaim, *Coord. Chem. Rev.*, 2002, **230**, 127; (b) D. Chavez and M. Hiskey, *J. Energ. Mater.*, 1999, **17**, 357.
- (a) A.-C. Knall and C. Slugovc, *Chem. Soc. Rev.*, 2013, **42**, 5131.
- (a) D. Boger, D. Soenen, C. Boyce, M. Hedrick and Q. Jin, *J. Org. Chem.*, 2000, **65**, 2479; (b) N. Saracoglu, *Tetrahedron.*, 2007, **63**, 4199; (c) S.-E. Suh, S. Barros and D. Chenoweth, *Chem. Sci.*, 2015, **6**, 5128.
- (a) I. Gural'skiy, D. Escudero, A. Frontera, P. Solnstev, E. Rusanov, A. Chernega, H. Kraustscheid and K. Domasevitch, *Dalton Trans.*, 2009, 2856; (b) P. Kar, M. Drew, C. Gómez-García and A. Ghosh, *Inorg. Chem.*, 2013, **52**, 1640; (c) C. Benso, A. Hui, K. Parimal, B. Cook, C.-H. Chen, R. Lord, A. Flood and K. Caulton, *Dalton Trans.*, 2014, **43**, 6513.
- T. Woods, M. Ballesteros-Rivas, S. Ostrovsky, A. Palii, O. Reu, S. Klokishner and K. Dunbar, *Chem. – Eur. J.*, 2015, **21**, 10302.
- D. Roberts, B. Pilgrim, J. Cooper, T. Ronson, S. Zarra and J. Nitschke, *J. Am. Chem. Soc.*, 2015, **137**, 10068.
- N. Shavaleev, S. Pope, Z. Bell, S. Faulkner and M. Ward, *Dalton Trans.*, 2003, 808.
- (a) L. Bogani and W. Wernsdorfer, *Nat. Mater.*, 2008, **7**, 179; (b) E. Coronado and M. Yamashita, *Dalton Trans.*, 2016, **45**, 16553; (c) Y. Wang, W. Li, S. Zhou, D. Kong, H. Yang and L. Wu, *Chem. Commun.*, 2011, **47**, 3541; (d) G. Cucinotta, M. Perfetti, J. Luzon, M. Etienne, P. Car, A. Caneschi, G. Calvez, K. Bernot and R. Sessoli, *Angew. Chem., Int. Ed.*, 2012, **51**, 1606; (e) Y.-N. Guo, G.-F. Xu, P. Gamez, L. Zhao, S.-Y. Lin, R. Deng, J. Tang and H.-J. Zhang, *J. Am. Chem. Soc.*, 2010, **132**, 8538.
- B. Rao, S. Dhokale, P. Rajamohanan and S. Hotha, *Chem. Commun.*, 2013, **49**, 10808.
- APEX Software Suite v.2012*, Bruker AXS, Madison, WI, 2005.
- R. Blessing, *Acta Crystallogr., Sect. A: Fundam. Crystallogr.*, 1995, **51**, 33.
- M. Schwach, H. Hausen and W. Kaim, *Inorg. Chem.*, 1999, **38**, 2242.
- D. Casanova, M. Llunel, P. Alemany and S. Alvarez, *Chem. – Eur. J.*, 2005, **11**, 1479.
- (a) F. Habib, G. Brunet, V. Vieru, I. Korobkov, L. Chibotaru and M. Murugesu, *J. Am. Chem. Soc.*, 2013, **135**, 13242; (b) F. Habib, P.-H. Lin, J. Long, I. Korobkov, W. Wernsdorfer and M. Murugesu, *J. Am. Chem. Soc.*, 2011, **133**, 8830; (c) P.-H. Lin, W.-B. Sun, Y.-M. Tian, P.-F. Yan, L. Ungur, L. Chibotaru and M. Murugesu, *Dalton Trans.*, 2012, **41**, 12349; (d) F. Yang, P. Yan, Q. Li, P. Chen and G. Li, *Eur. J. Inorg. Chem.*, 2012, 4287; (e) S.-Y. Lin, G.-F. Xu, L. Zhao, Y.-N. Guo and J. Tang, *Dalton Trans.*, 2011, **40**, 8213; (f) A. Gorczynski, M. Kubicki, D. Pinkowicz, R. Pelka, V. Patroniak and R. Podgajny, *Dalton Trans.*, 2015, **44**, 16833; (g) Y.-L. Chien, M.-W. Chang, Y.-C. Tsai, G.-H. Lee, W.-S. Sheu and E.-C. Yang, *Polyhedron*, 2015, **102**, 8; (h) P. Bag, C. Rastogi, S. Biswas, S. Sivakumar, V. Mereacre and V. Chandrasekhar, *Dalton Trans.*, 2015, **44**, 4328; (i) M. Holyńska, R. Clérac and M. Rouzières, *Chem. – Eur. J.*, 2015, **21**, 13321; (j) S. Xue, Y.-N. Guo, L. Ungur, J. Tang and L. Chibotaru, *Chem. – Eur. J.*, 2015, **21**, 14099; (k) C. Chen, J. Zhang, Y. Zhang, Z. Yang, H. Wu, G. Pana and Y. Bai, *J. Coord. Chem.*, 2015, **68**, 1054; (l) P.-H. Lin, W.-B. Sun, M.-F. Yu, G.-M. Li, P.-F. Yan and M. Murugesu, *Chem. Commun.*, 2011, **47**, 10993; (m) J.-P. Costes, F. Dahan and F. Nicodeme, *Inorg. Chem.*, 2003, **42**, 6556; (n) J. Chakraborty, A. Ray, G. Pilet, G. Chastanet, D. Luneau, R. Ziessel, L. Charbonnière, L. Carrella, E. Rentschler, M. Fallah and S. Mitra, *Dalton Trans.*, 2009, 10263; (o) F. Gao, Y.-Y. Li, C.-M. Liu, Y.-Z. Li and J.-L. Zuo, *Dalton Trans.*, 2013, **42**, 11043; (p) L. Natrajan, P. Timmins, M. Lunn and S. Heath, *Inorg. Chem.*, 2007, **46**, 10877; (q) P.-H. Lin, M. Leclère, J. Long, T. Burchell, I. Korobkov, R. Clérac and M. Murugesu, *Dalton Trans.*, 2010, **39**, 5698; (r) T. Balashova, A. Pushkarev, V. Ilichev, M. Lopatin, M. Katkova, E. Baranov, G. Fukin and M. Bochkarev, *Polyhedron*, 2013, **50**, 112; (s) V. Chandrasekhar, P. Bag, M. Speldrich, J. van Leusen and P. Kogerler, *Inorg. Chem.*, 2013, **52**, 5035; (t) X. Mei, X. Wang, J. Wang, Y. Ma, L. Li and D. Liao, *New J. Chem.*, 2013, **37**, 3620; (u) L. Zhao,

- J. Wu, H. Ke and J. Tang, *CrystEngComm*, 2013, **15**, 5301; (v) N. Anastasiadis, D. Kalofolias, A. Philippidis, S. Tzani, C. Raptopoulou, V. Psycharis, C. Milios, A. Escuer and S. Perlepes, *Dalton Trans.*, 2015, **44**, 10200; (w) Y.-C. Liu and Z.-Y. Yang, *Eur. J. Med. Chem.*, 2009, **44**, 5080; (x) J. Zhu, H.-F. Song, P.-F. Yan, G.-F. Hou and G.-M. Li, *CrystEngComm*, 2013, **15**, 1747; (y) H. Wang, C. Liu, T. Liu, S. Zeng, W. Cao, Q. Ma, C. Duan, J. Dou and J. Jiang, *Dalton Trans.*, 2013, **42**, 15355; (z) C.-J. Kuo, R. Holmberg and P.-H. Lin, *Dalton Trans.*, 2015, **44**, 19758.
- 15 (a) P.-H. Lin, T. Burchell, R. Clérac and M. Murugesu, *Angew. Chem., Int. Ed.*, 2008, **47**, 8848; (b) G. Brunet, F. Habib, I. Korobkov and M. Murugesu, *Inorg. Chem.*, 2015, **54**, 6195; (c) Y.-N. Guo, G.-F. Xu, W. Wernsdorfer, L. Ungur, Y. Guo, J. Tang, H.-J. Zhang, L. F. Chibotaru and A. K. Powell, *J. Am. Chem. Soc.*, 2011, **133**, 11948.
- 16 (a) Y.-C. Chen, J.-L. Liu, L. Ungur, J. Liu, Q.-W. Li, L.-F. Wang, Z.-P. Ni, L. Chibotaru, X.-M. Chen and M.-L. Tong, *J. Am. Chem. Soc.*, 2016, **138**, 2829; (b) J. Liu, Y.-C. Chen, J.-L. Liu, V. Vieru, L. Ungur, J.-H. Jia, L. Chibotaru, Y. Lan, W. Wernsdorfer, S. Gao, X.-M. Chen and M.-L. Tong, *J. Am. Chem. Soc.*, 2016, **138**, 5441; (c) M. U. Anwar, L. N. Dawe, S. S. Tandon, S. D. Bunge and L. K. Thompson, *Dalton Trans.*, 2013, **42**, 7781.
- 17 D. Pinkowicz, H. Southerland, C. Avendaño, A. Prosvirin, C. Sanders, W. Wernsdorfer, K. Pedersen, J. Dreiser, R. Clérac, J. Nehr Korn, G. Simeoni, A. Schnegg, K. Holldack and K. Dunbar, *J. Am. Chem. Soc.*, 2015, **137**, 14406.
- 18 W. Wernsdorfer, *Supercond. Sci. Technol.*, 2009, **22**, 064013.
- 19 N. Chilton, D. Collison, E. McInnes, R. Winpenney and A. Soncini, *Nat. Commun.*, 2013, **4**, 2551.
- 20 L. Ungur and L. Chibotaru, *Phys. Chem. Chem. Phys.*, 2011, **13**, 20086.